Numerical Heat Transfer, Part A: Applications: An International Journal of Computation and Methodology
Publication details, including instructions for authors and subscription information:
http://www.tandfonline.com/loi/unht20

HEAT TRANSFER ENHANCEMENT BY A MULTILOBE VORTEX GENERATOR IN INTERNALLY FINNED TUBES

Yeng-Yung Tsui, Shiann-Woei Leu
Published online: 29 Oct 2010.

To cite this article: Yeng-Yung Tsui, Shiann-Woei Leu (1999) HEAT TRANSFER ENHANCEMENT BY A MULTILOBE VORTEX GENERATOR IN INTERNALLY FINNED TUBES, Numerical Heat Transfer, Part A: Applications: An International Journal of Computation and Methodology, 35:5, 553-566, DOI: 10.1080/104077899275155

To link to this article: http://dx.doi.org/10.1080/104077899275155

Numerical Heat Transfer, Part A, 35:553–566, 1999

1040–7782/99 $12.00 + .00

HEAT TRANSFER ENHANCEMENT BY A MULTILOBE VORTEX GENERATOR IN INTERNALLY FINNED TUBES

Yeng-Yung Tsui and Shiann-Woei Leu
Department of Mechanical Engineering, National Chiao Tung University, Hsinchu 300, Taiwan, Republic of China

A three-dimensional computational method is employed to study the flow and heat transfer in internally finned tubes with a multilobe vortex generator inserted. Governing equations are discretized using the finite volume method. The irregular lobe geometry is treated using curvilinear nonstaggered grids. The linear interpolation method is adopted to calculate face velocities. The results show that secondary flows induced by the lobes are transformed to become axial vortices downstream of the vortex generator. As a consequence of the transport by the vortex flow, the core flow is moved to the fins and the tube wall, while the wall flow moves to the core. In this way, both heat transfer and flow mixing are enhanced. When the fin height is increased, the axial vortex is more restricted in the centerline region, and the strength of the vortex flow, represented by circulation, is decreased. In turn, the total pressure loss is also decreased. However, the heat transfer increases with fin height. Consequently, efficiency is greatly promoted.

INTRODUCTION

To augment heat transfer, internal fins are often employed in circular tubes. Such internally finned tubes have found wide usage in the design of compact heat exchangers and have been the subject of many studies [1–9]. When straight longitudinal fins are used, the flow field in the tubes is nearly undisturbed. The improvement of heat transfer is due to the increased wetted area introduced by the fins. With helical fins, a swirling flow is induced in the tube. The increase of heat transfer coefficient is then attributed not only to the increased area but also to the increased velocity near the tube wall and fins.

In addition to the surface modifications such as the internal fins described above, a variety of inserts have also been adopted as alternatives to enhance heat transfer. Among them, the twisted tape [10–13] is one of the most popular methods. Similar to the use of helical fins, a swirl is also induced in the tube by the twisted tape. The generation of the tangential velocity causes higher wall friction and thus higher heat transfer. However, the redistribution of flow temperature totally depends on the diffusion process in the swirling flow. This diffusion transport phenomenon is a slow process, especially for laminar flow.

Received 2 August 1998; revised 12 October 1998.

The authors wish to acknowledge support provided by the National Science Council under Contract NSC 87-2212-E009-038. The authors are also indebted to the National Center for High-Performance Computing for providing computer resources.

Address correspondence to Professor Yeng-Yung Tsui, Department of Mechanical Engineering, National Chiao Tung University, 1001 Ta Hsueh Road, Hsinchu, Taiwan 30050, Republic of China.

NOMENCLATURE

d	diameter of tube		ϕ directions ($= u/u_m, v/u_m, w/u_m$)
E	heat transfer enhancement factor	U_i	cylindrical velocity tensor
f	friction factor	W_i	contravariant velocity tensor
F	friction penalty factor	Z, R, ϕ	dimensionless cylindrical coordinates
h	lobe penetration		($= z/d, r/d, \phi$)
J	Jacobian of transformation	φ	dependent variable
l	length of the multilobe vortex	Γ	circulation
	generator	Γ_φ	diffusivity of φ
l_t	total tube length	η	efficiency index
Nu	Nusselt number	θ	dimensionless temperature
$\overline{\text{Nu}}$	mean Nusselt number		$[= (T - T_m)/(T_w - T_m)]$
P	dimensionless pressure ($= p/\rho u_m^2$)	ξ_i	curvilinear coordinates
Pr	Prandtl number ($= \nu/\alpha$)		
P_t	dimensionless total pressure		
Re	Reynolds number ($= u_m d/\nu$)	**Subscripts**	
S_φ	source term of the transport		
	equation for φ	b	bulk value
T	temperature	m	mean value at inlet
u_m	mean axial velocity	w	wall value
U, V, W	dimensionless velocities in z, r, and	0	empty tube value

In this study a multilobe vortex generator together with straight longitudinal fins are incorporated in a circular tube to improve heat transfer. The multilobe vortex generator, as shown in Figure 1, is a short tube with circular inlet but with convoluted trailing edge. As will be seen, when flow passes inside and outside of the lobes, radial and counterradial velocities are induced on both sides. These

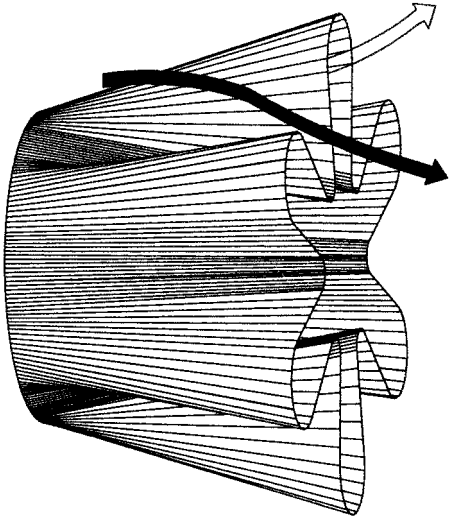

Figure 1. Schematic drawing of the multilobe vortex generator.

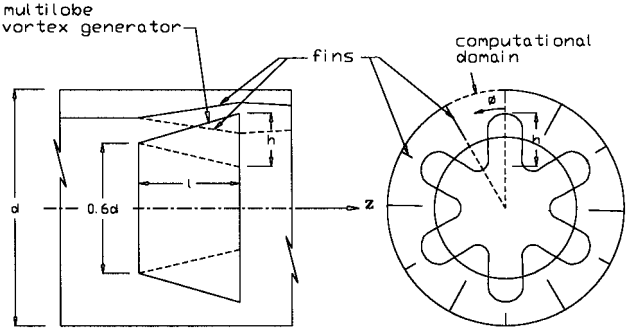

Figure 2. Configuration of the flow system.

secondary flows are transformed to become a number of axial vortices in the downstream region of the vortex generator. Theoretically, the number of vortices is 2 times the number of lobes. Carried by the vortices, the flow in the core region near the centerline is moved to the wall, and the flow near the wall to the centerline. Therefore it is expected that effective heat transfer and mixing of flow temperature can be obtained. This multilobe vortex generator has already been used in turbofan engines as an exhaust gas mixer such that the high-speed turbine flow stream can be mixed with the low-speed fan flow stream in a very short distance [14–17].

MATHEMATICAL METHOD

A schematic drawing of the tested flow configuration is shown in Figure 2. The flow is assumed to be steady, incompressible, and laminar. In order to fit the irregular geometry of the multilobe vortex generator, cylindrical coordinates are transformed onto curvilinear coordinates. The variables are nondimensionalized using tube diameter d and mean flow velocity u_m as characteristic length and velocity. The transport equations of momentum and energy can then be cast into the following form:

$$\frac{1}{JR}\frac{\partial}{\partial \xi_i}(W_i \varphi) = \frac{1}{JR}\frac{\partial}{\partial \xi_i}\left[\frac{\Gamma_\varphi}{JR}\left(\frac{\partial \varphi}{\partial \xi_j} B_j^i\right)\right] + S_\varphi \tag{1}$$

where φ stands for cylindrical coordinate velocity components U, V, W and dimensionless temperature θ. The tensor B_j^i is defined by

$$B_j^i = \beta_k^i \beta_k^j \tag{2}$$

Here

$$\beta_k^i = r_k \left(\text{cof}\frac{\partial Z_i}{\partial \xi_k}\right) \tag{3}$$

where the symbol cof($\partial Z_i/\partial \xi_k$) stands for the cofactor of $\partial Z_i/\partial \xi_k$ and

$$\begin{aligned} r_k &= R \qquad Z_i = Z, R \\ r_k &= 1 \qquad Z_i = \phi \end{aligned} \tag{4}$$

The contravariant velocities W_i are related to the cylindrical velocities U_i as

$$W_i = \beta_k^i U_k \tag{5}$$

In the flow system the thickness of the vortex generator and the fins is neglected. Since the lobes of the vortex generator and the fins are arranged in a periodic manner, the computational domain comprises a slice of half a lobe only. Symmetry boundaries are then imposed on the two side planes. At inlet the flow and temperature are assumed fully developed. The inlet temperature profile is given in Figure 3. Zero gradients are assumed at the outlet of the tube. No-slip condition is imposed on all solid walls, and constant temperature ($\theta = 1$) on the tube wall and fins.

Discretization of the governing equations is performed using the finite volume method by integrating the equations over each computational control volume. Convection terms are approximated by the linear upwind difference, and the diffusion terms by the central difference. It has been shown that with use of the second-order linear upwind difference scheme, numerical diffusion can be effectively suppressed [18].

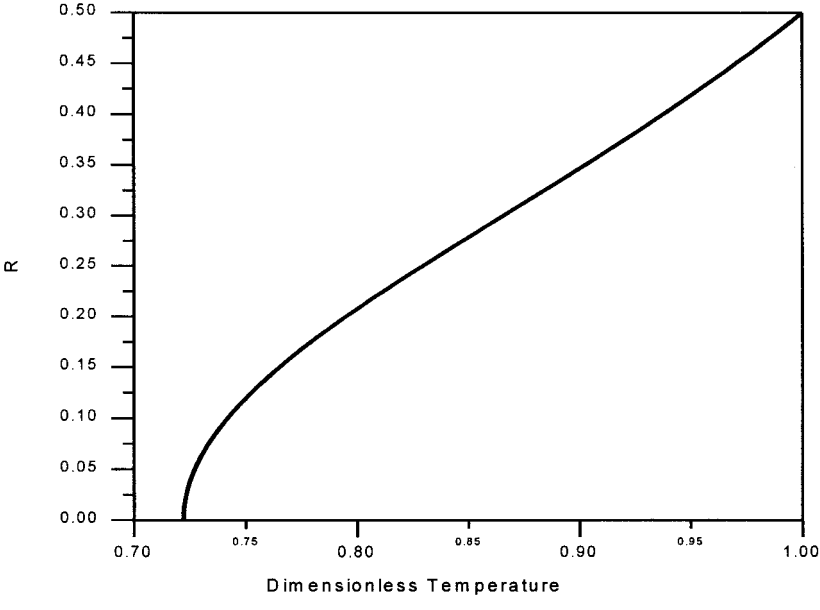

Figure 3. Fully developed inlet temperature profile.

The grids are arranged in a nonstaggered manner: all dependent variables are collocated at the cell centers. It is well known that this kind of grid arrangement may cause decoupling between velocity and pressure fields and thus checkerboard oscillation in solution. To avoid this problem, the momentum interpolation method of Rhie and Chow [19] is adopted to calculate the mass fluxes across the faces of each control volume. Following the SIMPLE algorithm [20], a pressure correction equation is then obtained by forcing the face velocities to satisfy the continuity constraint. Because of the use of curvilinear coordinates, 19 nodal points, 7 main nodes, plus 12 corner nodes are involved in the computational molecule of the pressure correction equation. During solution iteration, a common practice [21] is to drop the corner-point contributions such that the discrete equation is greatly simplified. However, as the grid skewness increases, the weighting of the corner points increases. The use of the above practice may prevent the solution from converging. Therefore the full 19-point pressure correction equation is used in this study.

Because of the complex lobe geometry, curvilinear three-dimensional (3-D) grids are necessitated. The grid is constructed by first generating 2-D grids at prescribed axial locations through solving a pair of elliptic-type partial differential equations [22]. After completing the 2-D grids, the corresponding grid points on all transverse planes are linked to form a 3-D grid. The grid lines along the axial direction might not be smooth. A smooth procedure is then undertaken. A typical grid generated by the above method is shown in Figure 4.

RESULTS AND DISCUSSION

To validate the above numerical procedure, the flow in a circular tube with different inserts studied by Fu and Tseng [23] was reproduced. Three kinds of inserts were tested: a short annular tube, a short sudden expansion tube, and a short sudden contraction tube. Comparison of the predicted Nusselt number Nu along the wall for the case of a short sudden contraction tube insert is shown in Figure 5. Close agreement between the two predictions is obtained, justifying the mathematical method.

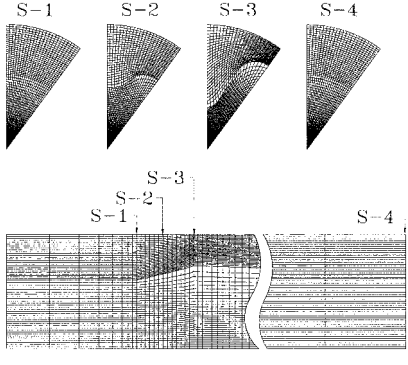

Figure 4. Computational grid.

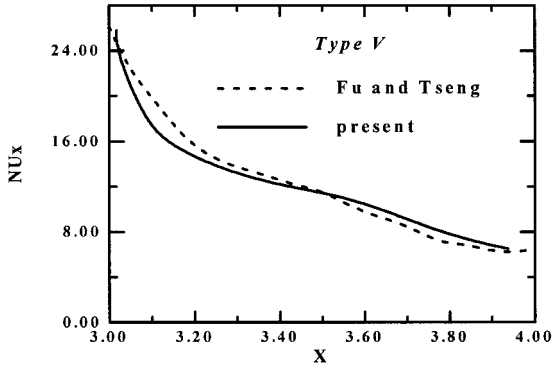

Figure 5. Comparison with the predictions of Fu and Tseng [23].

An assembly of the flow system tested in this study has been shown in Figure 2. A vortex generator comprising six lobes is inserted into a circular tube. A flow Reynolds number of 2000 is assumed and the Prandtl number is 5. The diameter of the vortex generator at its inlet is $0.6d$, while the length (l) is $1d$. The lobe penetration h at the trailing edge of the vortex generator is $0.212d$. The lobe contour geometry varies in a linear manner. The vortex generator is placed in the range between $0.5d$ and $1.5d$. The total length of the circular tube considered in the computations is $7d$. Twelve fins are installed on the inner wall of the circular tube. The fins are placed in the planes cutting through the lobe peaks and the lobe troughs. Because of the periodic arrangement of the lobes and fins, computations are restricted in a region of half a lobe, i.e., a slice of 30°. It is noted from Figure 2 that the heights of the fins are not constant. This is because in the calculation a number of grid spacings are assigned to the fins, and the grid spacing varies in the lobe region and downstream, as seen in Figure 4. Three fin heights, denoted as $0.25hf$, $0.5hf$, and $0.75hf$, were tested. As an example, $0.25hf$ means that the height of the fin in the region upstream of the inlet of the vortex generator is 0.25 times the height between the outer tube and the inlet edge of the vortex generator.

Grid refinement tests have been done for the case of the $0.5hf$ fin. Four grid levels, ranging from 22,500 to 120,000 nodal points, were used. The resulting circulation and total pressure loss, which will be defined below, are presented in Figures 6 and 7. It is seen that the predictions for the two finest grids are close to each other. It is the finest grid, $80(Z) \times 60(R) \times 25(\phi)$, that is used in the results presented in the following.

Velocity vector plots on axial and diametral planes for the $0.25hf$ and $0.75hf$ are given in Figures 8 and 9. The axial plane $\phi = 0°$ is the symmetry boundary on the peak side of the lobe, while the $\phi = 30°$ plane is the boundary on the trough side. It is seen from the axial planes that when the flow goes through the lobe, it follows the lobe surface without causing separation. However, as seen in the diametral planes, secondary velocities are induced in the lobe region due to the convoluted shape. A radially upward velocity toward the peak is formed inside the lobe, and a radially downward velocity toward the trough is formed outside

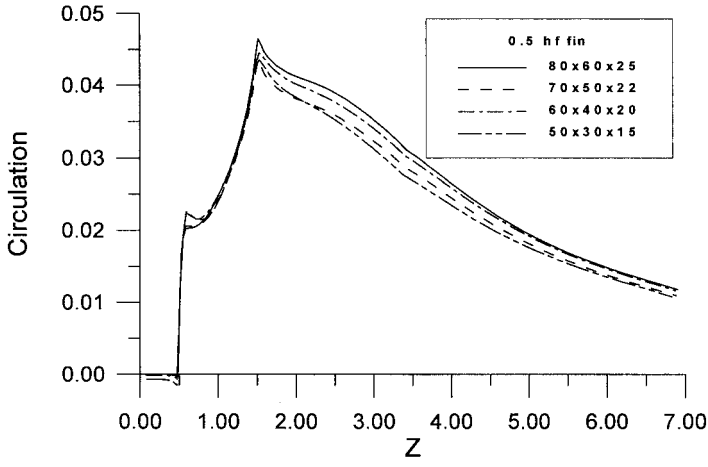

Figure 6. Variation of circulation for grid refinement tests.

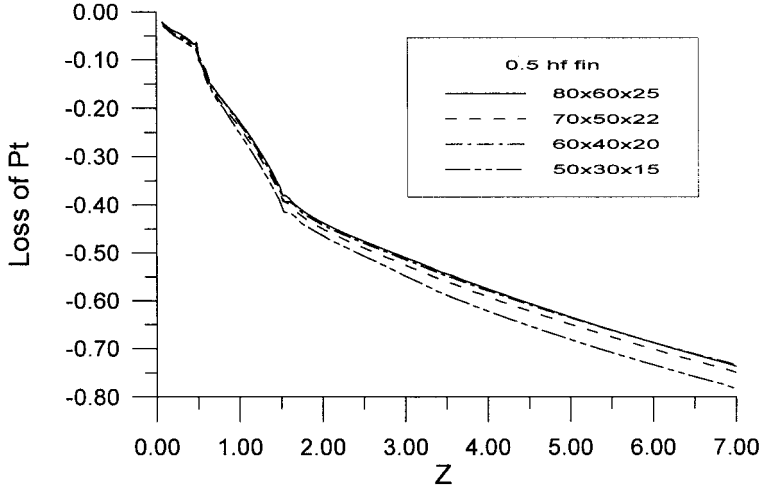

Figure 7. Variation of total pressure loss for grid refinement tests.

the lobe. The flow pattern is even complicated for the 0.75*hf* case, in which small vortices appear in the corners formed by the tube wall and the fins. After the flow emerges from the lobe, the radial and counterradial flow structure is transformed to become an organized axial vortex. This vortex occupies most of the diametral planes, especially for the 0.25*hf* case due to its short fins, and persists to the exit of the tube. Because of viscous dissipation, the strength of the vortex flow gradually attenuates, which can be identified from the magnitude scale. It is noted that the strength of the induced secondary flow is greater for the 0.25*hf* case. Since the inlet velocity and temperature are assumed fully developed, the axial velocity is large, and the temperature is small in the core region near the centerline. The

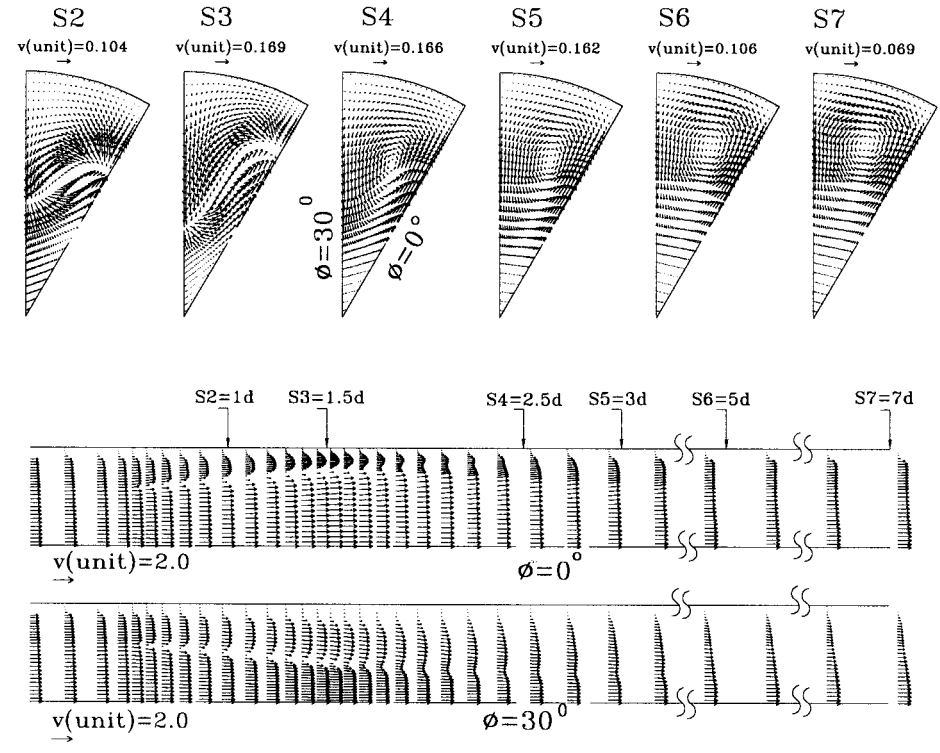

Figure 8. Velocity vectors in diametral and axial planes for the 0.25*hf* fin case.

high-speed, low-temperature core flow is transported by the vortex to sweep across the fins and the tube wall such that heat exchange takes place there. The temperature distributions in diametral planes for the two cases are shown in Figures 10 and 11. The curved isotherms indicate that the low-speed, high-temperature wall flow is transported by the vortex away from the wall to mix with the high-speed, low-temperature core flow. In this way, effective heat transfer as well as mixing of flow are obtained.

It has been seen that the axial vortex is the most significant character in the flow field. The strength of the vortex can be quantified by introducing the circulation,

$$\Gamma = \oint_C \mathbf{V} \cdot d\mathbf{s} \tag{6}$$

where the circuit C denotes the outer path of the considered domain in a diametral plane, i.e., the path comprising the two symmetry lines, the fins, and the tube wall. Since velocity vanishes on the tube wall and the fins, the circulation is equal to the line integral of the radial velocity along the two symmetry boundaries. The variation of circulation along the axis for the three fin cases and the case

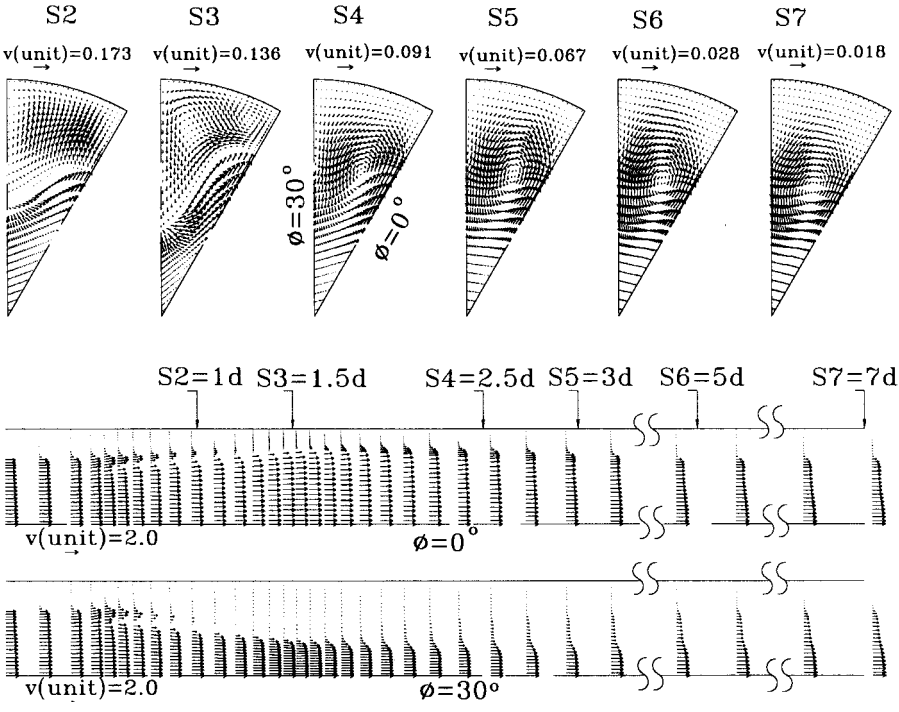

Figure 9. Velocity vectors in diametral and axial planes for the 0.75*hf* fin case.

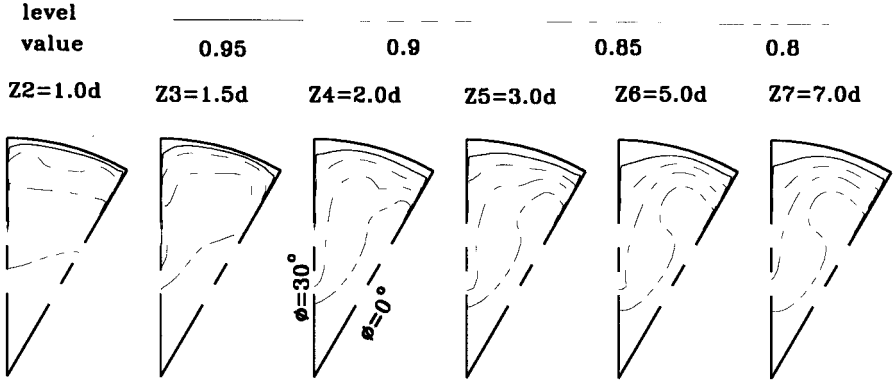

Figure 10. Isotherms in diametral planes for the 0.25*hf* fin cases.

Figure 11. Isotherms in diametral planes for the 0.75*hf* fin case.

without fins is shown in Figure 12. The circulation builds up in the lobe and reaches its peak at the end of the lobe. Owing to viscous dissipation, it attenuates gradually, as illustrated in the figure. The appearance of the fins restricts the development of the axial vortex, resulting in lower circulation for the fin cases. It has been shown in the vector plots that the vortex is mainly in the centerline region away from the corners surrounded by the tube wall and the fins. The higher the fins are, the smaller the circulation is.

The variation of Nu along the tube wall is shown in Figure 13. Nu is defined as

$$\mathrm{Nu} = \frac{\int_0^{\phi_{\max}} (\partial\theta/\partial R)|_{\mathrm{wall}}\, d\phi}{(1-\theta_b)\phi_{\max}} \tag{7}$$

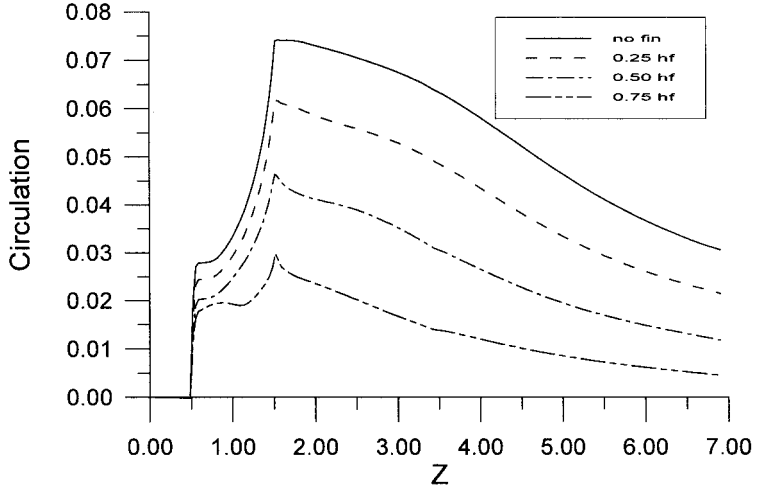

Figure 12. Axial variation of circulation.

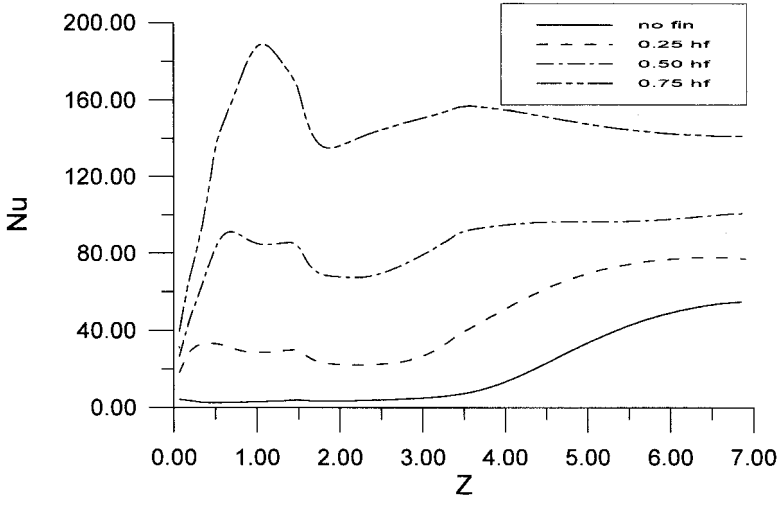

Figure 13. Axial variation of Nusselt number.

where θ_b is the bulk temperature,

$$\theta_b = \frac{\int_A U\theta \, dA}{\int_A U \, dA} \tag{8}$$

Nu quickly increases from the tube inlet for the fin cases because, initially, there exists large temperature gradients between the flow and the fins. The high heat transfer in the lobe region is sustained by the secondary flow induced by the lobe. After the flow escapes from the lobe, Nu decreases first, followed by an augmentation. This heat transfer enhancement is attributed to the transport of the high-speed, low-temperature core flow by the vortex to sweep over the fins and the tube wall. In spite of the weakest circulation for the $0.75hf$ case, it has the greatest heat transfer because its fin area is large.

Accompanied by the improvement of heat transfer, pressure loss is inevitably also enlarged. The variation of loss of total pressure is given in Figure 14. The total pressure, defined below, is based on a flux-averaged form:

$$P_t = \frac{\int_A U(P + (1/2)U^2) \, dA}{\int_A U \, dA} \tag{9}$$

where only the axial velocity component is considered in the dynamic pressure. It is noted from the figure that the pressure loss for the $0.75hf$ fin case is the highest. However, the loss for the $0.25hf$ and $0.5hf$ cases is even lower than that for the case without fins. The cause of the lower loss for the cases with low fin heights is due to their weaker vortex flow and, as seen before, the vortex is away from the fins and tube wall, leading to lower wall friction.

The performances of the considered cases are summarized in Table 1. In this table, $\overline{\mathrm{Nu}}$ stands for the Nusselt number averaged over the entire tube wall, and f

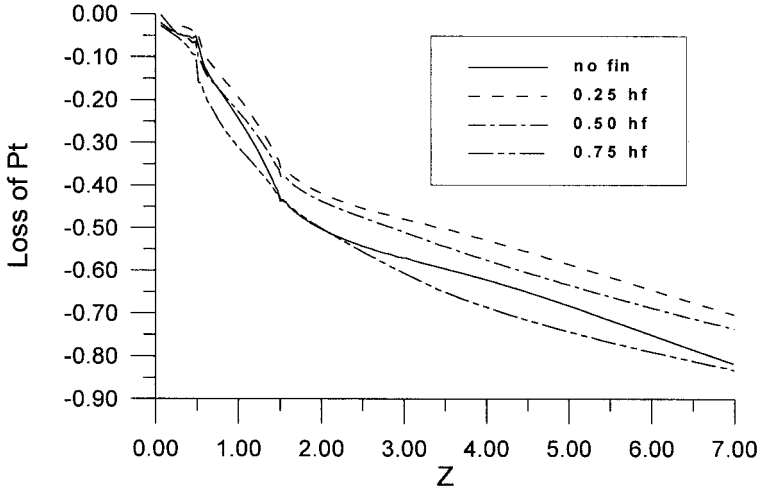

Figure 14. Axial variation of total pressure loss.

Table 1. Heat transfer enhancement factor, friction penalty factor, and efficiency index for tested cases

Fin configuration	$\overline{\mathrm{Nu}}$	$f(\times 10^{-2})$	E	F	η
No fin	20.	11.7	5.5	3.7	1.5
0.25*hf*	48.3	10.	13.2	3.1	4.2
0.5*hf*	86.6	10.5	23.7	3.3	7.2
0.75*hf*	145.7	11.9	39.8	3.7	10.7

is the friction factor, defined as

$$f = \frac{\Delta P}{(1/2)U_m^2}\frac{d}{l_t} \tag{10}$$

where ΔP is the pressure drop between the tube inlet and tube outlet. E and F are the heat transfer enhancement factor and the friction penalty factor, respectively, defined by

$$E = \frac{\overline{\mathrm{Nu}}}{\mathrm{Nu}_0} \tag{11}$$

$$F = \frac{f}{f_0} \tag{12}$$

where Nu_0 and f_0 denote the Nusselt number and friction factor, respectively, of a

fully developed laminar flow in a smooth empty tube. Theoretically,

$$\mathrm{Nu}_0 = 3.66 \tag{13}$$

$$f_0 = \frac{64}{\mathrm{Re}} \tag{14}$$

Finally, the parameter in the last column of Table 1 represents the efficiency index:

$$\eta = \frac{E}{F} \tag{15}$$

which is used to evaluate the quality of enhancement. Comparing with the case without fins, the heat transfer is greatly improved by the appearance of the fins. The mean Nusselt number and heat enhancement factor increase with the fin height. However, it should be noted that the pressure loss and thus the friction penalty factor are not increased due to the fact that the induced vortex flow is weaker and away from the tube wall, as discussed above. Therefore the efficiency index is largely increased as the fin height increases.

CONCLUSIONS

A three-dimensional numerical procedure has been adopted to examine the flow and heat transfer in internally finned tubes with a multilobe vortex generator inserted. Based on the results, the following conclusions can be drawn.

1. The secondary velocities induced by the lobes are transformed to become axial vortices in the region downstream of the lobe. The appearance of the fins restricts the development of the vortex flow, resulting in lower circulation.
2. When the vortex is well developed at a distance downstream of the lobe, the heat transfer is greatly enhanced mainly because of the transport of the high-speed, low-temperature core flow by the vortex to sweep across the wall and the fins. Also, owing to the convection transport of the vortex flow, the high-temperature wall flow is quickly mixed with the low-temperature core flow.
3. With the use of fins, the heat transfer is largely improved. However, the pressure loss is not increased, especially for the cases with low fin heights. This is attributed to the fact that the induced vortex is more concentrated in the centerline region and is weaker. As a consequence of the increased heat transfer and decreased pressure loss, the efficiency index is largely increased. This index increases with fin height.

REFERENCES

1. S. V. Patankar, M. Ivanovic, and E. M. Sparrow, Analysis of Turbulent Flow and Heat Transfer in Internally Finned Tubes and Annuli, *ASME J. Heat Transfer*, vol. 101, pp. 29–37, 1979.

2. R. L. Webb and M. J. Scott, A Parametric Analysis of the Performance of Internally Finned Tubes for Heat Exchanger Application, *ASME J. Heat Transfer*, vol. 102, pp. 38–43, 1980.
3. H. M. Soliman, T. S. Chau, and A. C. Trupp, Analysis of Laminar Heat Transfer in Internally Finned Tubes with Uniform Outside Wall Temperature, *ASME J. Heat Transfer*, vol. 102, pp. 598–604, 1980.
4. G. J. Rowley and S. V. Patankar, Analysis of Laminar Flow and Heat Transfer in Tubes with Internal Circumferential Fins, *Int. J. Heat Mass Transfer*, vol. 27, pp. 553–560, 1984.
5. C. Prakash and Y.-D. Liu, Analysis of Laminar Flow and Heat Transfer in the Entrance Region of an Internally Finned Circular Duct, *ASME J. Heat Transfer*, vol. 107, pp. 84–91, 1985.
6. I. M. Rustum and H. M. Soliman, Numerical Analysis of Laminar Forced Convection in the Entrance Region of Tubes with Longitudinal Internal Fins, *ASME J. Heat Transfer*, vol. 110, pp. 310–313, 1988.
7. I. M. Rustum and H. M. Soliman, Experimental Investigation of Laminar Mixed Convection in Tubes with Longitudinal Internal Fins, *ASME J. Heat Transfer*, vol. 110, pp. 366–372, 1988.
8. W. J. Marner and A. E. Bergles, Augmentation of Highly Viscous Laminar Heat Transfer Inside Tubes with Constant Wall Temperature, *Exp. Thermal Fluid Sci.*, vol. 2, pp. 252–267, 1989.
9. R. L. Webb, *Principles of Enhanced Heat Transfer*, John Wiley, New York, 1994.
10. E. Smithberg and F. Landis, Friction and Forced Convection Heat-Transfer Characteristics in Tubes with Twisted Tape Swirl Generators, *ASME J. Heat Transfer*, vol. 86, pp. 39–49, 1964.
11. R. F. Lopina and A. E. Bergles, Heat Transfer and Pressure Drop in Tape-Generated Swirl Flow of Single-Phase Water, *ASME J. Heat Transfer*, vol. 91, pp. 434–442, 1969.
12. A. W. Date, Prediction of Fully Developed Flow in a Tube Containing a Twisted Tape, *Int. J. Heat Mass Transfer*, vol. 17, pp. 845–859, 1974.
13. N. S. Gupte and A. W. Date, Friction and Heat Characteristics of Helical Turbulent Air Flow in Annuli, *ASME J. Heat Transfer*, vol. 111, pp. 337–344, 1989.
14. P. Koutmos and J. J. McGuirk, Turbofan Forced Mixer/Nozzle Temperature and Flow Field Modeling, *Int. J. Heat Mass Transfer*, vol. 32, pp. 1141–1153, 1989.
15. D. C. McCormick and J. C. Bennett Jr., Vortical and Turbulent Structure of a Lobed Mixer Free Shear Layer, *AIAA J.*, vol. 32, pp. 1852–1859, 1994.
16. Y.-Y. Tsui and P.-W. Wu, Investigation of the Mixing Flow Structure in Multilobe Mixers, *AIAA J.*, vol. 35, pp. 1386–1391, 1996.
17. R. W. Paterson, Turbofan Mixer Nozzle Flow Field—A Benchmark Experimental Study, *ASME J. Eng. Gas Turbines Power*, vol. 106, pp. 692–698, 1984.
18. Y.-Y. Tsui, A Study of Upstream-Weighted High-Order Differencing for Approximation to Flow Convection, *Int. J. Numer. Methods Fluids*, vol. 13, pp. 167–199, 1991.
19. C. M. Rhie and W. L. Chow, A Numerical Study of the Turbulent Flow Past an Isolated Airfoil with Trailing Edge Separation, *AIAA J.*, vol. 21, pp. 1525–1532, 1983.
20. S. V. Patankar, *Numerical Heat Transfer and Fluid Flow*, McGraw-Hill, New York, 1980.
21. M. Peric, Analysis of Pressure-Velocity Coupling on Nonorthogonal Grids, *Numer. Heat Transfer, Part B*, vol. 17, pp. 63–82, 1990.
22. J. L. Steger and R. L. Sorenson, Automatic Mesh-Point Clustering near a Boundary in Grid Generation with Elliptic Partial Differential Equations, *J. Comput. Phys.*, vol. 33, pp. 405–410, 1979.
23. W.-S. Fu and C.-C. Tseng, Enhancement of Heat Transfer for a Tube with an Inner Tube Insertion, *Int. J. Heat Mass Transfer*, vol. 37, pp. 499–509, 1994.